

Mechanical Properties of UNS S39274 Superduplex Stainless Steel Work Hardened and Solution Annealed

J.N. Conceição^a, E.O. Correa^a , A.C. Gonzaga^b, J. M. Parda^{b,c}, S.S.M. Tavares^{b,c,*} 

^aUniversidade Federal de Itajubá, Programa de Pós-Graduação em Materiais para Engenharia, Itajubá, MG, Brasil.

^bCentro Federal de Educação Tecnológica Celso Suckow da Fonseca, Programa de Pós-Graduação em Engenharia Mecânica e Tecnologia de Materiais, Rio de Janeiro, RJ, Brasil.

^cUniversidade Federal Fluminense, Rua Passo da Pátria, 156, 24210-240, Niterói, RJ, Brasil.

Received: March 06, 2022; Revised: April 25, 2022; Accepted: May 11, 2022

UNS S39274 is a W-alloyed superduplex stainless steel used in critical services in the oil and gas production. This material was selected for tubulars used in oil country tubular goods, below the Christmas tree. In order to achieve high mechanical strength the seamless tubes are cold drawn in a costly operation. In this work the mechanical properties of a cold drawn seamless were characterized and compared to three solution treated materials. Tensile curves were obtained and modelled by Hollomon's, Ludwik's and Voce's models, where the last one presented the higher correlation coefficients in all cases. The hardness and impact toughness at -46°C were measured and discussed. The results were analyzed taking into account the microstructural changes produced by cold drawing and annealing.

Keywords: *superduplex stainless steel, solution annealing, mechanical properties.*

1. Introduction

Superduplex stainless steels (SDSSs) are austenitic-ferritic corrosion resistant alloys (CRA) with pitting resistance equivalent number (PREN) higher than 40¹. This class of steels combines high strength and corrosion resistance with a competitive cost, when compared Ni alloys². For these reasons SDSSs have found widespread use in chemical and petrochemical industries, specially in the oil and gas production and refining².

UNS S32750 and UNS S32760 are traditional grades of SDSS with 25%Cr, 7%Ni and 3-4%Mo (wt.%). Both grades have significant nitrogen contents (~0.25%N), and the difference is the small additions of Cu (0.5-1.0%) and W (0.5-1.0%) in the UNS S32760. A newly developed and less popular grade UNS S39274 has the same base composition of Cr, Ni, Mo and N, but higher W addition (1.5-2.5%). W is a δ -stabilizing element which increases the mechanical resistance by solid solution strengthening, and also improves the localized corrosion resistance³⁻⁵. In the UNS S39274 steel the W addition allows a small reduction of the Mo content to the range of 2.5-3.5%. For steels containing W the pitting resistant equivalent number shall be calculated as: $PREN_W = \%Cr + 3.3(\%Mo + 0.5(\%W)) + 16(\%W)$.

One of the noble applications of UNS S39274 in the petrochemical industry is in seamless pipes for casings and tubulars, also called oil country tubular goods (OCTG). High pressure and high temperatures (HP/HT) wells with aggressive environments (i.e., high H₂S and/or CO₂ dissolved gases) are becoming more and more common⁶. Oilfield downhole tubulars were usually made of high

strength low alloy (HSLA) steels. However, under severe operating conditions, such as high temperature, high pressure and solutions containing CO₂ and H₂S, corrosion failures are likely to occur. Under such harsh conditions it is necessary to consider the use of corrosion resistant alloys (CRAs). In a crescent order of cost and corrosion resistance, the most indicated CRAs are 13Cr martensitic stainless steels, supermartensitic stainless steels, duplex (DSS) and superduplex stainless steels (SDSS), and nickel alloys⁷. SDSSs have higher corrosion resistance with a lower cost than nickel alloys, but the mechanical resistance in the annealed condition is lower than the values achieved by supermartensitic stainless steels. Thus, work hardening is used as strengthening mechanism to increase the yield limit, and values as high as 862 MPa (125 ksi) may be achieved, while in the solution treated (annealed) condition the material has 552 MPa (80 ksi) minimum. Work hardening of heavy seamless tubes is applied by cold drawn, a very costly process made by a very few numbers of manufacturers.

In this work the mechanical properties of a seamless tube of W-alloyed UNS S39274 SDSS were investigated. The effect of solution treatment in three different temperatures (1050 °C, 1100 °C and 1150 °C) was evaluated and compared to the as received-cold worked condition.

2. Materials and Methods

The material studied was W-alloyed SDSS type UNS S39274 from a seamless tube with outside diameter 169.0 mm and wall thickness 10.0 mm. The chemical composition and the PREN of the steel are shown in Table 1.

*e-mail: ssmtavares@terra.com.br

The as received tubular has been cold worked to achieve the mechanical properties of Grade 125 – of ISO 13680 standard⁸. Parts of the tube were cut and roughly machined to approximate dimensions of tensile tests and subsize Charpy impact tests. All specimens were longitudinal, as shown in Figure 1. The outlines were solution treated (ST) at three different temperatures, 1050 °C, 1100 °C, and 1150 °C, with water cooling. The specimens in this work were identified as AR-CW (as received-cold worked), ST-1050, ST-1100 and ST-1150. After the heat treatments the materials were machined to the final dimensions of tensile specimens (gauge length 16 mm and diameter 4.0 mm), and subsize V-notched Charpy specimens (55 x 10 x 7.5 mm).

Simulations of the volume fraction of the equilibrium phases present in the three solution treatment temperatures were performed and the equilibrium chemical compositions in each phase were determined with *Thermo-Calc*[®] computer program package and TCFE6 database.

Microstructural characterization was performed by optical and scanning electron microscopies (OM and SEM) in order to determine the austenite and ferrite volume fractions, and to evaluate qualitatively the chromium nitride precipitation. The specimens were etched with Behara's etching (20 ml HCl, 80 ml distilled H₂O and 0.3 g K₂S₂O₅) for phase quantification. Etchs with 10% oxalic acid solution (electrolytic, 9.0 V, 60 s) and 40% HNO₃ solution (electrolytic, 1.1 V, 60 s) were used to reveal chromium nitrides.

Tensile tests were performed with velocity 0.5 mm/minute in an Instron servo-mechanical machine with 100 kN of capacity. The nominal stress (σ_N) versus nominal strain (ϵ_N)

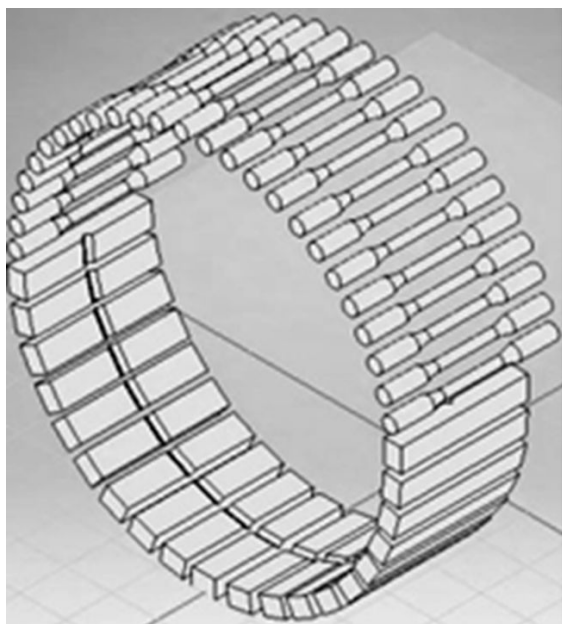


Figure 1. Specimens orientation as respect to the seamless tube.

curves and true stress (σ) versus true strain (ϵ) curves were obtained. Tensile tests were performed in duplicate for each heat treatment condition.

For each condition it was obtained a $\sigma \times \epsilon$ average curve, considering the two respective stress-strain curves of the samples. The points representing the sample's stress-strain curves were rearranged to obtain the same points along its strain (X-axis), according to Equation 1:

$$x_n = \frac{\sum_{i=1}^k P_n^i}{k} \quad (1)$$

Where n is the number of values obtained in the tension tests and k is the number of specimens evaluated for each condition. For each specimen, the stress values (Y-axis) resulting from the rearranged strain points were linearly approximated based on their respective acquisition points⁹.

Three mathematical models were tested to describe σ versus ϵ curves^(10,11,12):

$$\sigma = K_H \epsilon^{n_H} \quad (2)$$

$$\sigma = \sigma_o + K_L \epsilon^{n_L} \quad (3)$$

$$\sigma = \sigma_o + P_1 \epsilon_T + P_2 (1 - \exp(-P_3 \epsilon_T)) \quad (4)$$

Where σ and ϵ are the true stress and true strain, respectively; σ_o is the tensile point where plastic deformation starts; K_H , K_L , n_H , n_L , P_1 , P_2 and P_3 are parameters to be determined in the models.

Charpy impact tests were performed at -46°C in a universal pendul with maximum capacity 300J. The specimens were examined after the test in the scanning electron microscope in a *FEI Inspect S50 model*, with tungsten filament operating at high vacuum (approximately 1.56×10^{-2} Pa), beam voltage between 20 and 30 kV and with secondary electron detectors for high vacuum operation (ETD/SE).

Vickers hardness tests with load 10 kgf were performed in the cross section of the tube. Vickers microhardness with 25 gf was measured in ferrite and austenite phases, also in the plane of the cross section of the pipe.

3. Results and Discussion

Figures 2a, b show the microstructures revealed with Behara's etching. Table 2 shows the results of phase quantification obtained by quantitative metallography (ASTM E-562¹³) and compares with the equilibrium phase amounts predicted with *Thermo-Calc*[®]. Table 3 presents the equilibrium chemical compositions and PREN values of each phase obtained by thermodynamic simulation (*Thermo-Calc*[®]). The increase of the solution temperature increases the equilibrium ferrite content and this trend was observed in the optical microscopy analysis. However, *Thermo-Calc*[®] predicted 1.69% of sigma phase at 1050 °C, but no traces of this phase were detected by optical nor scanning electron microscopy.

Table 1. Chemical composition (wt%) and PREN of the UNS S39274 SDSS studied.

C	Cr	Ni	Mo	W	Cu	S	P	N	Fe	PREN
0.028	24.790	6.600	3.220	1.750	0.510	0.002	0.017	0.255	Bal.	42.40

Figures 3a-c show the intense attack in the ferrite phase and in δ/γ boundaries of solution treated specimens, provoked by the electrolytic etching with 10% oxalic acid solution (9.0 V, 60 s). This etch corrodes the areas surrounding chromium nitrides and carbides. According to Knyazeva and Pohl¹⁴ quenched-in nitrides correspond to metastable CrN, while Petterson et al.¹⁵ demonstrated that both CrN and Cr₂N are present in SDSS type UNS S32750 fast cooled from high temperature (1250 °C).

Chromium nitride quantification is a difficult task, and it was not performed in this work. However, the comparison between Figures 3a, b and c shows qualitatively that the increase of solution temperature increases the amount of quenched-in chromium nitrides resulted after cooling.

Specimen ST-1150 have all ferrite grains attacked, while specimen ST-1050 have only some grains corroded, and specimen ST-1100 show an intermediate behaviour. Another interesting comparison is made between specimens ST-1050 and ST-1150 etched with 40% HNO₃ solution (1.1 V, 60 s), with a larger CrN/Cr₂N density in the ferrite of ST-1150 (Figures 4a, b). The explanation is that the increase of solution temperature raises the ferrite content (Table 2) and the nitrogen concentration in the ferrite. To corroborate this, the equilibrium solubility of nitrogen in the ferrite phase was estimated with *Thermo-Calc*[®] (Table 3), and corresponds to 0.0314%, 0.0416% and 0.0546% for 1050 °C, 1100 °C and 1150 °C, respectively. Quenched-in nitrides precipitate in the ferrite because the solubility of nitrogen in this phase

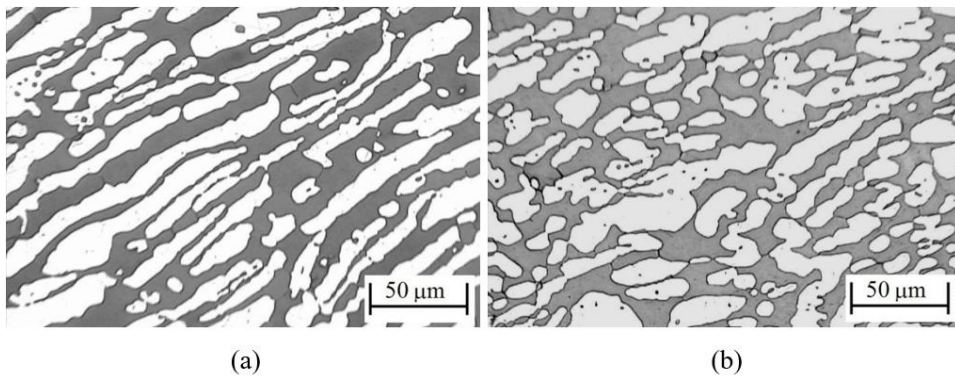


Figure 2. Microstructures of the steels in the cross section: (a) as received (AR-CW); (b) ST-1150.

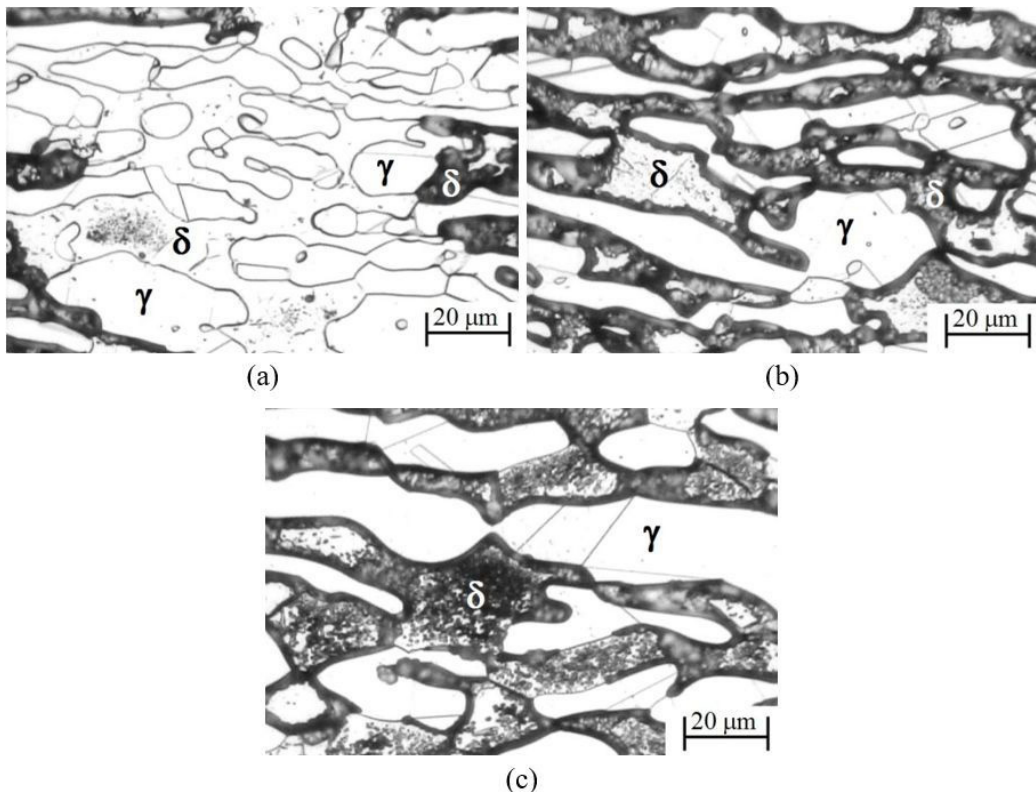


Figure 3. Specimens etched with 10% acid oxalic solution (9.0 V, 60 s): (a) ST-1050; (b) ST-1100; (c) ST-1150.

decreases abruptly below 1000 °C, and even cooling rates as high as 2500 °C/s cannot avoid precipitation inside ferrite grains and in ferrite/austenite boundaries¹³

Table 4 compares the hardness and microhardness results. There is no significant variation of hardness with solution treatment temperature in the interval investigated (1050 – 1150 °C), despite of the slight increase of microhardness of both phases with the decrease of solution temperature. It is also worth noting that the increase of chromium nitrides in the ferrite with the increase of solution temperature did not increase the microhardness of this phase, as could be supposed from previous researches^{16,17}.

Before cold drawing the pipe was solution treated, probably in a temperature into the 1050 – 1125 °C range,

according to the ASTM A790¹⁸. It is interesting to note that in the solution treated condition the microhardness of ferrite is superior to that of austenite. Cr, Mo and W promote solid solution strengthening of ferrite, while nitrogen is a strong strengthener of austenite. After the solution treatment in the tube manufacturer, in a rough estimative based on the results of Table 4, the ferrite and austenite microhardness were close to 300 HV10 and 250 HV10, respectively. After cold drawing the microhardness of austenite became higher than that of ferrite, which means that austenite has higher work hardenability than ferrite in the UNS S39274 SDSS. Austenitic steels have higher work hardenability than ferritic ones because the FCC austenite has 12 symmetric slip systems composed by supercompact planes ($\{111\}$),

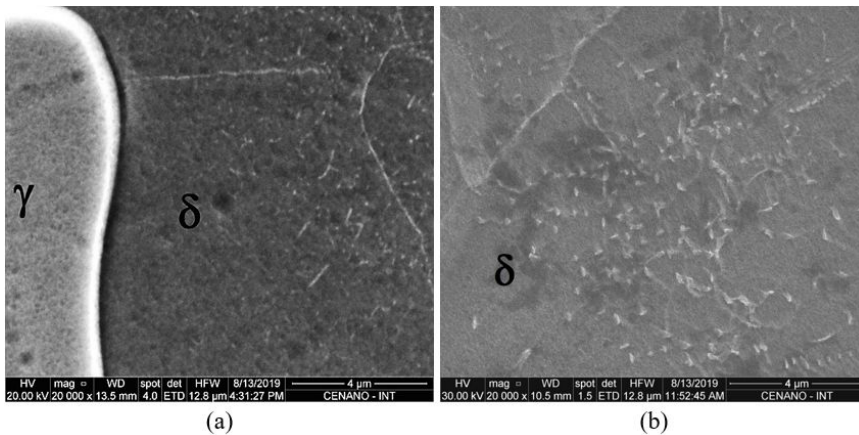


Figure 4. Specimens etched with 40% HNO₃ solution (1.1 V, 60 s): (a) ST-1050; (b) ST-1150.

Table 2. Phase volume fractions of phases determined by quantitative metallography (ASTM E-562¹³) and by simulation (*Thermo-Calc*[®]).

Specimen	Quantitative metallography		Simulation prediction (solution temperature)		
	% austenite (γ)	% ferrite (δ)	% austenite (γ)	% ferrite (δ)	% sigma (σ)
AR-CW	56.1 ± 7.2	43.9 ± 7.2	-	-	-
ST-1050	60.8 ± 8.5	39.2 ± 8.5	56.4	41.9	1.7
ST-1100	52.4 ± 5.1	47.6 ± 5.1	50.9	49.1	0.0
ST-1150	51.3 ± 4.9	48.7 ± 4.9	45.6	54.4	0.0

Table 3. Equilibrium contents (wt%) and PREN_w values of each phase obtained by simulation (*Thermo-Calc*[®]).

T(°C)	Phase	Cr	Ni	Mo	W	N	C	PREN _w
1050	Ferrite (δ)	26.638	4.682	3.903	2.143	0.0314	0.0079	43.56
	Austenite (γ)	23.202	8.133	2.460	1.314	0.4272	0.0476	40.32
1100	Ferrite (δ)	26.271	4.975	3.935	2.136	0.0416	0.0088	43.45
	Austenite (γ)	23.310	8.223	2.506	1.364	0.4641	0.0512	41.26
1150	Ferrite (δ)	25.936	5.250	3.828	2.058	0.0546	0.0099	42.84
	Austenite (γ)	23.369	8.274	2.467	1.369	0.4990	0.0549	41.75

Table 4. Vickers hardness and microhardness of ferrite and austenite phases.

Specimen	Vickers Hardness (HV10)	Microhardness (HV0.025)	
		Ferrite (δ)	Austenite (γ)
AR-CW	(344 ± 7)	323 ± 20	331 ± 16
ST-1050	(281 ± 9)	317 ± 15	265 ± 11
ST-1100	(285 ± 5)	299 ± 16	257 ± 11
ST-1150	(279 ± 2)	273 ± 11	246 ± 10

while BCC ferrite have 48 possible slip systems, but none of them have supercompact planes and, hence, a lot of them are inoperant at low temperatures. Interestingly, this feature was also observed in the biphasic microstructure of austenite and ferrite of the SDSS.

Figures 5a and 5b compare the nominal stress (σ_N) versus nominal strain (ϵ_N) and true stress (σ_T) versus true strain (ϵ_T) average curves, respectively. Table 5 presents the mechanical properties extracted from the σ_N versus ϵ_N curves. The AR-CW condition has a significantly higher yield (960 MPa) and ultimate strength (1007 MPa) than solution treated ST-1050, ST-1100 and ST-1150, with lower ductility parameters, as expected. Comparing solution treatment temperatures, specimens ST-1100 and ST-1150 presents very similar tensile curves and properties, while ST-1050 has slight higher ductility parameters. At increased solution annealing temperatures, like 1150 °C, as shown in Table 2, the lowest austenite volume fraction leads to a lower elongation and reduction of area, and in this way, the highest austenite content displays the most desirable mechanical properties, when considering the three solution annealing temperatures aforementioned. The nitrogen is a strong austenite stabilizer and influences the ferrite and austenite phase distribution. Besides, the nitrogen content in the ferrite phase is increased

by raising the temperature, which increases the susceptibility to nitride formation during rapid cooling^{15,19}.

The curves σ versus ϵ were modelled by Equations 2, 3 and 4. Figures 6a and 6b compares the three models with experimental data of specimens AR-CW(A) and ST-1050(A) respectively. Table 6 shows the parameters obtained in the fittings, with respective correlation coefficients R^2 .

The strain hardening exponents (n_H and n_L) and the strength coefficient (K_H and K_L) are parameters in Hollomon's (Equation 2) and Ludwik's (Equation 3) models, where n_H and n_L measure the persistence of hardening and K_H and K_L are related to the level of strength that the material can withstand^{20,21}. Strain hardening describes the increase of stress necessary to continue deformation at any stage of plastic strain and it is explained on the basis of dislocation-dislocation strain field interactions. The strain-hardening exponent may have values from $n = 0$ (perfectly plastic solid) to $n = 1$ (elastic solid). For most metals n has values between 0.10 and 0.50²². As a tendency, high-strength materials have lower n values, like the cold worked AR-CW steel, in comparison to lower strength materials, like in all solution annealed treated specimens (ST-1050, ST-1100 and ST-1150). With a low n , the work hardening rate is initially high, but the rate decreases quickly with strain. On the other

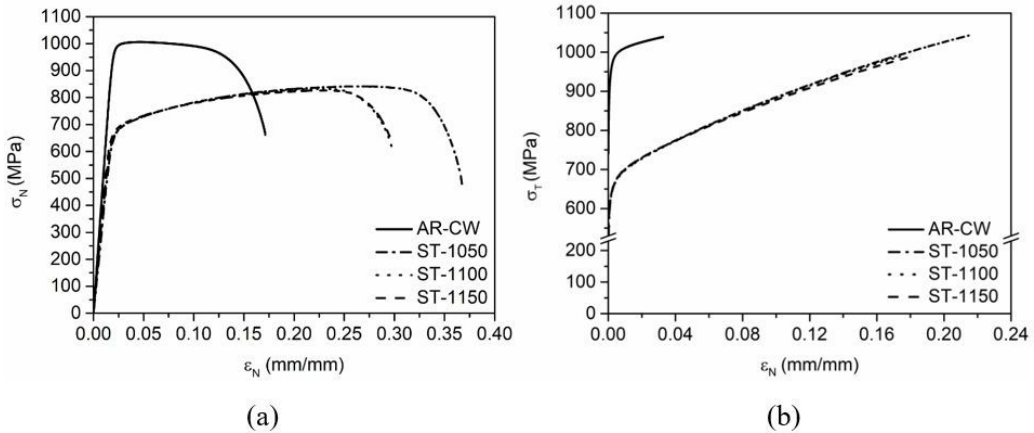


Figure 5. Average curves from tensile tests: (a) nominal stress (σ_N) versus nominal strain (ϵ_N); (b) true stress (σ_T) versus true strain (ϵ_T).

Table 5. Tensile properties (two tests per condition, average values are also reported).

Tensile Properties	Specimen									
	AR-CW		ST-1050		ST-1100		ST-1150			
	(A)	(B)	(A)	(B)	(A)	(B)	(A)	(B)		
σ_{YS} (MPa)	947	974	628	641	609	652	632	646		
	(960 ± 19)		(634 ± 9)		(630 ± 30)		(639 ± 10)			
σ_{UTS} (MPa)	999	1014	842	841	831	841	824	833		
	(1007 ± 10)		(842 ± 0)		(836 ± 8)		(829 ± 6)			
Elongation (%)	Plastic		19.1	16.2	35.7	36.5	35.4	28.8	28.6	35.2
			(17.7 ± 2.1)		(36.1 ± 0.6)		(32.1 ± 4.7)		(31.9 ± 4.6)	
	Uniform		5.3	4.1	26.31	28.04	27.4	21.3	21.9	27.6
		(4.7 ± 0.9)		(27.2 ± 1.2)		(24.4 ± 4.3)		(24.7 ± 4.0)		
Reduction of Area (%)	78.3	74.7	81.5	83.0	81.6	82.3	80.4	73.9		
	(76.5 ± 2.6)		(82.2 ± 1.1)		(82.0 ± 0.5)		(77.2 ± 4.6)			
$\sigma \times \epsilon$ Area (10^{12} J/m ³)	178.2	151.3	279.5	287.8	272.4	225.0	221.0	276.9		
	(164.7 ± 19.0)		(283.7 ± 5.9)		(248.7 ± 33.5)		(249.0 ± 39.5)			

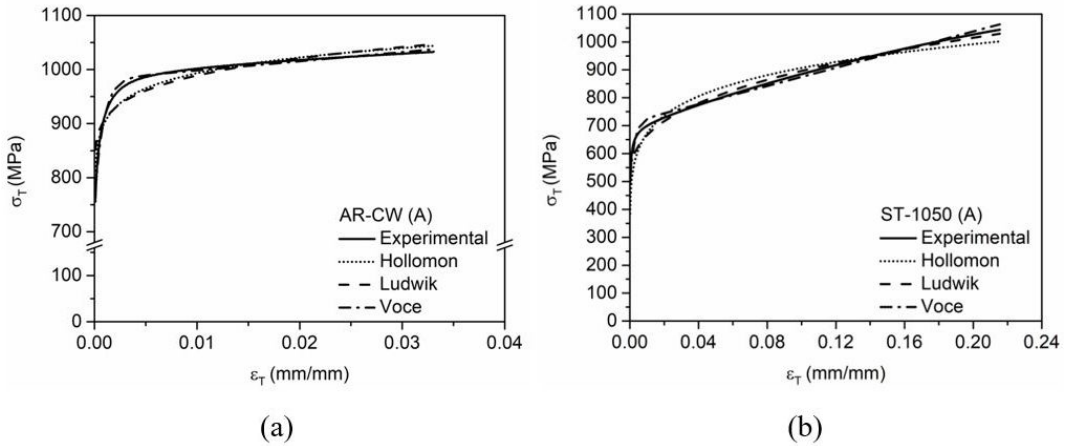


Figure 6. True stress-strain curves of specimens (a) AR-CW (A) and (b) ST-1050 (A), with the three Hollomon's, Ludwik's and Voce's models.

Table 6. Hollomon's, Ludwik's and Voce's models of the flow curves σ versus ϵ results.

Model	Specimen								
	AR-CW		ST-1050		ST-1100		ST-1150		
	(A)	(B)	(A)	(B)	(A)	(B)	(A)	(B)	
Hollomon	K_H (MPa)	1202.7 (1220.8 ± 25.7)	1239.0	1222.0 (1223.0 ± 1.4)	1224.0	1225.0 (1193.6 ± 44.4)	1162.2	1151.6 (1176.7 ± 35.5)	1201.8
	n_H	0.042 (0.042 ± 0.001)	0.043	0.130 (0.129 ± 0.001)	0.129	0.139 (0.123 ± 0.023)	0.107	0.113 (0.118 ± 0.007)	0.124
	R^2	0.930	0.939	0.929	0.862	0.859	0.881	0.922	0.915
Ludwik	σ_0 (MPa)	755 (764 ± 13)	773	499 (505 ± 8)	510	533 (543 ± 14)	553	510 (524 ± 19)	537
	K_L (MPa)	546.4 (582.0 ± 50.3)	617.5	944.8 (944.7 ± 0.1)	944.6	1001.9 (929.0 ± 103.2)	856.0	867.5 (884.3 ± 23.8)	901.1
	n_L	0.184 (0.194 ± 0.014)	0.203	0.376 (0.382 ± 0.009)	0.388	0.470 (0.427 ± 0.061)	0.384	0.365 (0.386 ± 0.029)	0.406
	R^2	0.865	0.870	0.985	0.934	0.939	0.841	0.986	0.986
Voce	σ_0 (MPa)	755 (764 ± 13)	773	499 (505 ± 8)	510	533 (543 ± 14)	553	510 (524 ± 19)	537
	P_1 (MPa)	1697.1 (2005.4 ± 436.0)	2313.7	1629.7 (1605.8 ± 33.8)	1581.9	1622.0 (1641.9 ± 28.1)	1661.8	1661.5 (1578.4 ± 117.5)	1495.2
	P_2 (MPa)	226.3 (222.7 ± 5.1)	219.1	212.8 (209.1 ± 5.3)	205.4	159.7 (167.1 ± 10.5)	174.5	192.4 (188.4 ± 5.7)	184.4
	P_3	1179.5 (1317.3 ± 194.9)	1455.2	375.4 (400.4 ± 35.3)	425.4	226.7 (281.6 ± 77.6)	336.5	412.4 (368.0 ± 62.8)	323.5
	R^2	0.993	0.992	0.992	0.990	0.993	0.991	0.992	0.993

hand, in a high n , the initial work hardening is less rapid but remains to high strains²¹. In Figures 6a and 6b it is noted the effect of n on the shape of the curves, with the AR-CW (A) (lower n) showing an almost horizontal shape and the ST-1050 (A) presenting a steeper curve. Comparing only the solution annealing steels, the highest average n_H values were 0.129 (ST-1050), followed by 0.123 (ST-1100) and 0.118 (ST-1150), in the Hollomon's model. In the Ludwik's model the highest average n_L value was 0.427 (ST-1100), followed by 0.386 (ST-1150) and 0.382 (ST-1050).

The Voce's law is an isotropic hardening model employed to characterize the elasto-plastic region of the tensile test results commonly applied for materials with little hardening and high

plasticity, like steels which exhibit a saturating hardening behavior. This Voce's law is indicated in Equation 3, where σ_0 is the proportional limit and ϵ is the true plastic strain of the material. P_1 (stiffness coefficient), P_2 (strain hardening coefficient) and P_3 (strain hardening exponent) are other hardening parameters^{9,21}. Comparing the results in Table 6, the Voce's law simulations of plastic behavior had the best fitting precision, with R^2 (coefficient of determination) values ranging from 0.990 to 0.993, whereas Hollomon and Ludwik models presented R^2 values from 0.859 to 0.939 and from 0.841 to 0.986, respectively.

From Table 6, the average values of proportional limit (σ_0) are higher in AR-CW (764 MPa) and lower in ST-1100

(543 MPa), ST-1150 (524 MPa) and ST-1050 (505 MPa). The average stiffness coefficient (P_1), which controls the hardening rate, is higher in AR-CW (2005.4 MPa), followed by ST-1100 (1641.9 MPa), ST-1050 (1605.8 MPa) and ST-1150 (1578.4 MPa). The average strain hardening coefficient (P_2) is related to the difference between the proportional limit and the yield strength of the material, and the highest values were in AR-CW (222.7 MPa), followed by ST-1050 (209.1 MPa), ST-1150 (188.4 MPa) and ST-1100 (167.1 MPa). The average strain hardening exponent (P_3) influences the elasto-plastic transition curvature, and the highest value was in AR-CW (1317.3), followed by ST-1050 (400.4), ST-1150 (368.0) and ST-1100 (281.6). Summarising, all parameters of the Voce's equation were higher in as-received cold worked (AR-CW) specimen.

SEM micrographs of the fracture surface of tensile specimens AR-CW (B) (Figures 7a-c), ST-1050 (B) (Figures 7d-f)

and ST-1100 (B) (Figures 7g-i) showed the occurrence of many micro-dimples and dimple fracture characteristics in all materials. In addition, there are some dimples and a fibrous network on the border fracture surfaces, which is characterized by a ductile fracture. The fracture surface has an elliptical shape, as already observed in a DSS UNS S32205 hot rolled tube²³. This seems to be a typical behaviour of seamless tubes, due to their anisotropic microstructure.

Charpy V-notch impact tests were performed in all materials and the results are shown in Table 7. The fracture morphologies observed by SEM after the impact tests are presented in Figures 8a-c for specimen AR-CW(A), Figures 8d-f for ST-1100 (B) and Figures 8g-i for ST-1150.

In all specimens the absorbed energy, lateral expansion (Table 7) and fractographic aspect are typical from ductile or shear type failures, with the lowest average value obtained in the specimens treated at 1150 °C (165.5 J). This is slightly

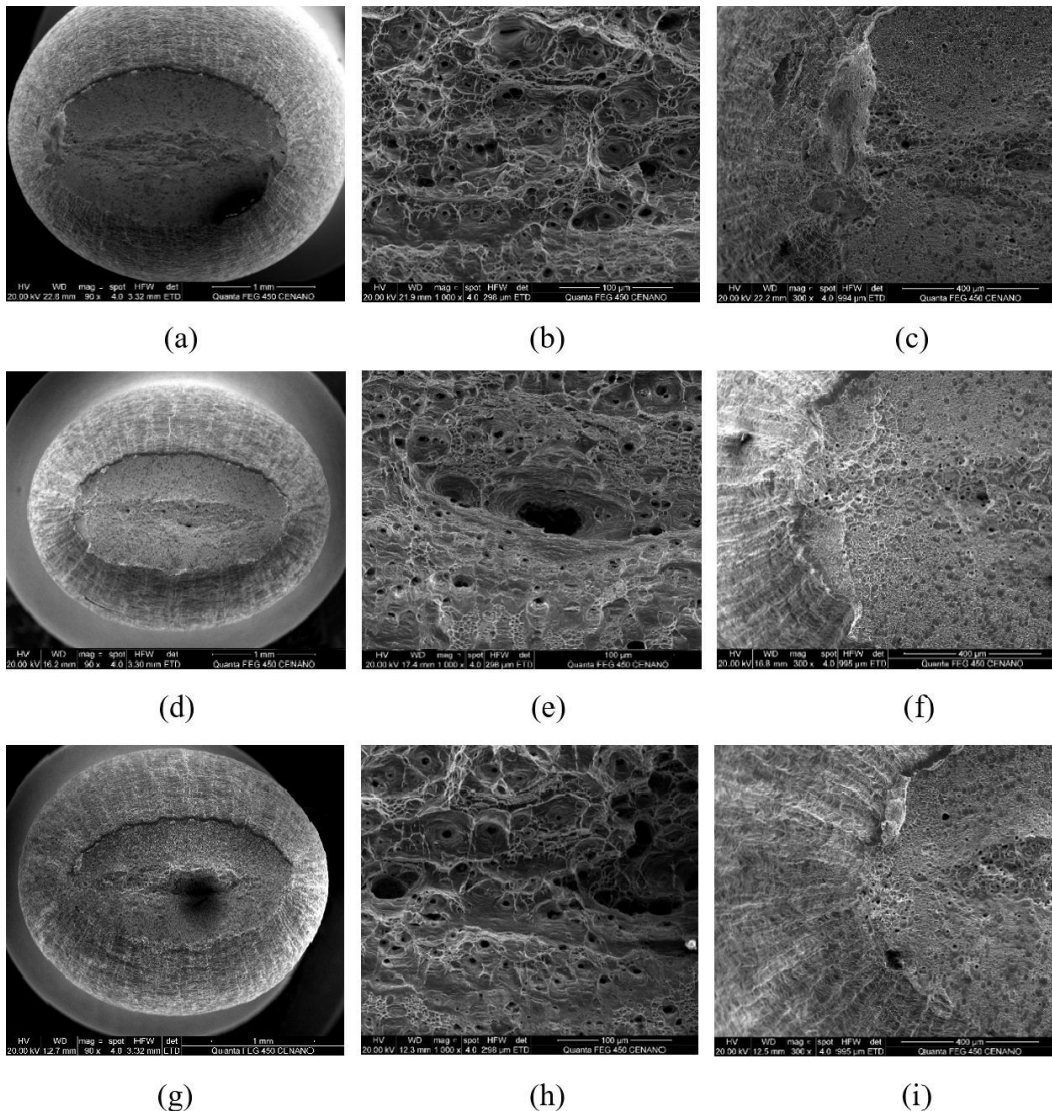


Figure 7. Fractography observed by SEM of tensile specimens: (a), (b) and (c) AR-CW(B); (d), (e) and (f) ST-1050(B); (g), (h) and (i) ST-1100(B).

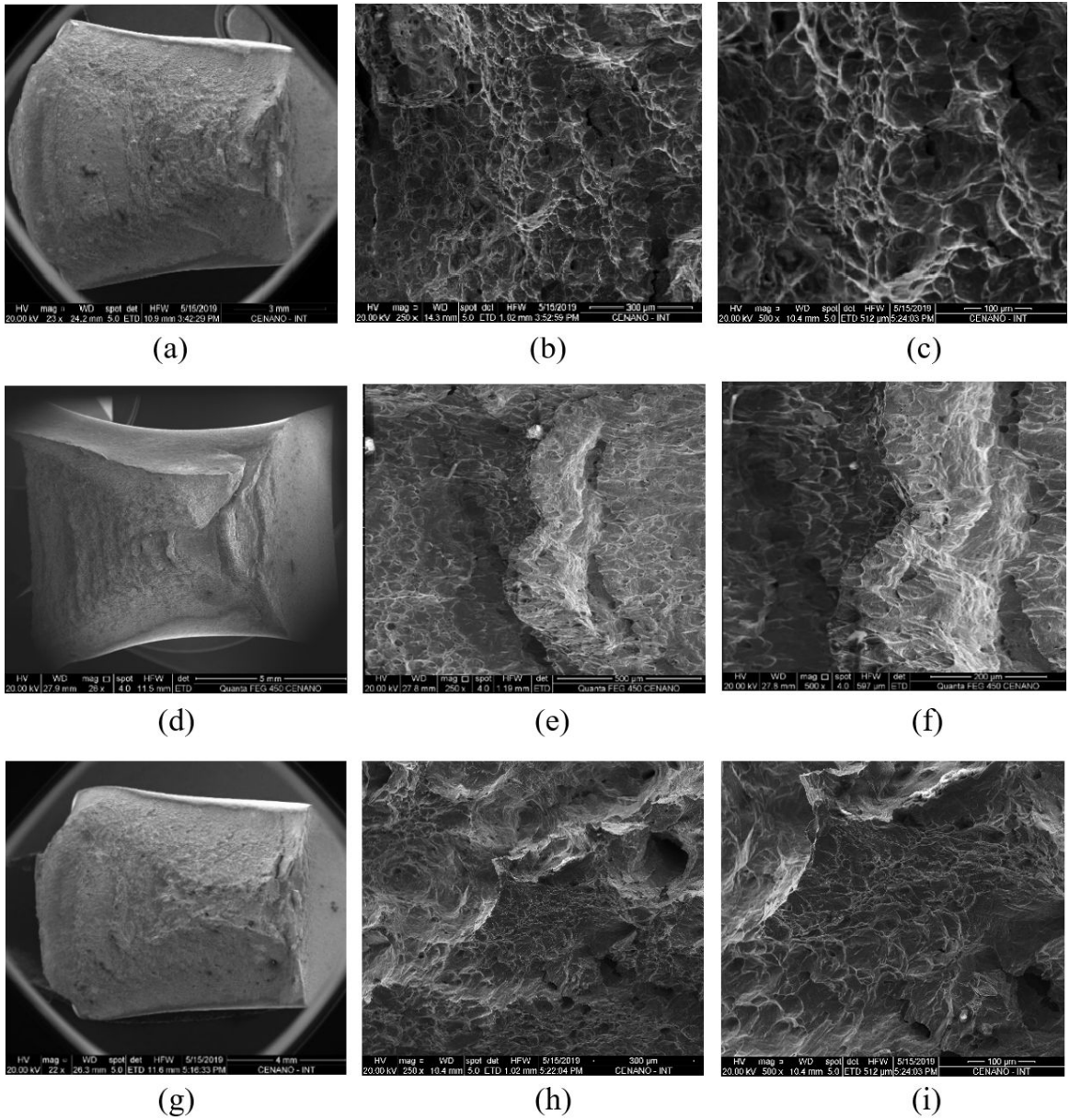


Figure 8. SEM micrographs showing the fracture surface morphology after Charpy impact testing at -46°C : (a), (b) and (c) AR-CW (A); (d), (e) and (f) ST-1100 (B); (g), (h) and (i) ST-1150 (A).

Table 7. Charpy V-notched Impact test at -46°C results.

Specimen	Absorbed Energy (J)		Lateral Expansion (mm)		Shear Fracture (%)	
	Tests	Avg	Tests	Avg	Tests	Avg
AR-CW (A)	172.0	(170.5 ± 2.1)	2.24	(2.21 ± 0.04)	75	(71.0 ± 5.7)
AR-CW (B)	169.0		2.18		67	
ST-1050 (A)	269.0	(265.5 ± 17.7)	2.51	(2.52 ± 0.01)	86	(84.5 ± 2.1)
ST-1050 (B)	244.0		2.53		83	
ST-1100 (A)	294.0	(294.0 ± 0.0)	2.59	(2.42 ± 0.25)	94	(94.5 ± 0.7)
ST-1100 (B)	294.0		2.24		95	
ST-1150 (A)	179.0	(165.5 ± 19.1)	2.20	(2.04 ± 0.23)	72	(69.0 ± 4.2)
ST-1150 (B)	152.0		1.88		66	

lower than the average impact toughness of specimens as received (AR-CW) (170.5 J). Although SDSS are rarely employed at -46 °C, this test temperature is frequently adopted, as in the reference standard NORSOK M-630²⁴. The minimum values specified by this standard for subsize specimens are 37.5 J for average values and 28J for single specimens. The cold deformation has probably decreased the impact toughness, but the minimum and average values of AR-CW condition were largely superior to the minimum required. As regard to the specimens ST-1150, their lower values compared to the other solution temperatures (1100°C and 1050°C) may be attributed to its higher ferrite content and to the Cr nitrides precipitates. According to Ramirez et al.²⁵, these particles reduce the mobility of dislocations. Although the results of this work show that Cr₂N/CrN nitrides does not harden the steel, the decrease of impact toughness observed in specimens ST-1150 indicates that these precipitates have an embrittlement effect.

4. Conclusions

The mechanical properties of a cold worked tube of superduplex stainless steel UNS S39274 were investigated and compared to solution treated materials. The main conclusions are:

- Cold work of the tube (drawing) was able to increase the yield limit and ultimate strength to 947 MPa and 973MPa, respectively, with significant decrease of total and uniform elongations. On the other hand, the reduction of area in the tensile test of cold worked tube was similar to the solution treated specimens. In all cases, the fracture surface was ductile and with elliptical shape.
- The impact toughness of the cold drawn pipe measured at -46 °C was 170.5 J (sub-size specimen). This result proves that cold working is an interesting hardening mechanism for superduplex UNS S39274 steel, since it was able to increase the yield stress by a factor higher than 1.5 maintaining a very high toughness.
- The tensile curves of the specimens cold worked, and cold worked and annealed at 1050 °C, 1100 °C and 1150 °C were modelled by Hollomon's, Ludwik's, and Voce's equations, with better correlation coefficients obtained in the last one.
- The increase of solution treatment from 1050 °C to 1150 °C resulted in a microstructure with higher ferrite phase, and higher amount of Cr nitrides precipitated. These particles do not harden the ferrite phase, but probably have some detrimental effect on the impact toughness.

5. Acknowledgments

Authors acknowledge to Brazilian research agencies CAPES, CNPq and FAPERJ for financial support, and CENANO/INT for the SEM analysis.

6. References

1. ISO: International Organization for Standardization. ISO 15156/NACE 0175 - Petroleum, petrochemical, and natural gas industries - Materials for use in H2S-containing environments in oil and gas production - Part 3: Cracking-resistant CRAs (corrosion resistant alloys) and other alloys. Geneva: ISO; 2015.
2. Yousefieh M, Shamanian M, Saatchi A. Influence of step annealing temperature on the microstructure and pitting corrosion resistance of SDSS UNS S32760 welds. *J Mater Eng Perform*. 2011;20(9):1678-83.
3. Ha H-Y, Lee T-H, Kim S. Effect of W on stress corrosion cracking susceptibility of newly developed Ni-saving duplex stainless steels. *Met Mater Int*. 2017;23(1):115-25.
4. Haugan EB, Naess M, Rodriguez CT, Johnsen R, Iannuzzi M. Effect of tungsten on the pitting and crevice corrosion resistance of type 25Cr super duplex stainless steels. *Corrosion*. 2017;73(1):53-67.
5. Park C-J, Kwon H-S. Effects of aging at 475°C on corrosion properties of tungsten-containing duplex stainless steels. *Corros Sci*. 2002;44:2817-30.
6. Cao S, He F, Gao J. Corrosion problems in the oil country tubular goods and their mitigation – a review. *Anti-Corros Methods Mater*. 2017;64(5):465-78.
7. Francis R. The role of duplex stainless steels for downhole tubulars. In: 25th Annual Offshore Technology Conference; 1993; Houston, Texas, USA. Proceedings. Vienna: IAEA; 1993. p. 577-87.
8. ISO: International Organization for Standardization. ISO 13680 - Petroleum and natural gas industries — Corrosion-resistant alloy seamless tubular products for use as casing, tubing, coupling stock and accessory material — Technical delivery conditions. Geneva: ISO; 2020.
9. Chales R, Cardoso ASM, Parda JM, Tavares SSM, Silva MM, Reis DAP. Modeling and numerical validation of stress-strain curves of maraging steels, grades 300 and 350 under hydrogen embrittlement. *Mater Res*. 2021;24(3):e20200431.
10. Ludwik P. *Elemente der technologischen mechanik*. Berlin: Springer; 1909.
11. Hollomon JH. Tensile deformation. *Trans AIME*. 1945;162:268-90.
12. Kraft SM, Gordon AP. Characterization of the behavior of a metallic fiber woven structure. *Text Res J*. 2011;81:1249-72.
13. ASTM International. ASTM E-562-19e1, Standard Test Method for Determining Volume Fraction by Systematic Manual Point Count. West Conshohocken, PA, USA: ASTM International; 2019.
14. Knyazeva M, Pohl M. Duplex steels. Part II: carbides and nitrides. *Metallogr Microstruct Anal*. 2013;2:343-51.
15. Pettersson NL, Pettersson RFA, Wessman S. Precipitation of chromium nitrides in the super duplex stainless Steel 2507. *Metall Mater Trans, A Phys Metall Mater Sci*. 2015;46:1062-72.
16. Hereñú S, Moscato MG, Alvarez I, Armas AF. The influence of chromium nitrides precipitation on the fatigue behavior of duplex stainless steels. *Procedia Eng*. 2014;74:179-82.
17. Horvath W, Tabernig B, Werner E, Uggowitzer P. Microstructures and yield strength of nitrogen alloyed superduplex stainless steel. *Acta Mater*. 1997;45:1645-54.
18. ASTM International. ASTM A-790-20: Standard Specification for Seamless and Welded Ferritic/Austenitic Stainless Steel Pipe. West Conshohocken, PA, USA: ASTM International; 2020.
19. Hengsbach F, Koppa P, Duschik K, Holzweissig MJ, Burns M, Nellesen J, et al. Duplex stainless steel fabricated by selective laser melting - Microstructural and mechanical properties. *Mater Des*. 2017;133:136-42.
20. Nutor RK, Adomako NK, Fang YZ. Using the hollomon model to predict strain-hardening in metals. *Am J Mater Synth Process*. 2017;2(1):1-4.
21. Hosford WF. *Mechanical behavior of materials*. 2nd ed. New York: Cambridge University Press; 2010. p. 65-68.

22. Dieter GE. Mechanical metallurgy. Singapore: McGraw Hill; 1988. p. 287-8.
23. Barros TS, Pecly PHR, Parda JM, Gonzaga AC, Tavares SSM. Comparison between hot rolled and powder metallurgy–Hot Isostatic Pressing (PM-HIP) processed duplex stainless steel UNS S32205. *J Mater Eng Perform*. <http://dx.doi.org/10.1007/s11665-022-06616-8>.
24. NORSOK Standards. NORSOK M-630: Material data sheets and element data sheets for piping. 6th ed. Oslo, Norway: NORSOK Standards; 2013.
25. Ramirez AJ, Lippold JC, Brandi SD. The relationship between chromium nitride and secondary austenite precipitation in duplex stainless steels. *Metall Mater Trans, A Phys Metall Mater Sci*. 2003;34A:1575-97.